Tool-Path Planning Method For Kinematics Optimization of Blade Machining On Five-Axis Machine Tool

Zhongyang Lu
Jilin University
Xu Yang (yangxu@jlu.edu.cn)
Jilin University School of Mechanical and Aerospace Engineering
Ji Zhao
Jilin University

Research Article

Keywords: Tool-path planning, Aero-engine blade, Kinematics optimization, Conformal transformation, Free-form surface

Posted Date: January 5th, 2022

DOI: https://doi.org/10.21203/rs.3.rs-1213345/v1

Abstract

Planning tool-paths on free-form surfaces is a widely discussed issue. However, traditional methods of generating paths capable of meeting all the requirements of blade machining remain challenging. In this study, a new iso-parametric path-planning strategy based on a novel parameterization method combined with the conformal transformation theory was proposed. The proposed method could adapt to the curvature characteristics of the blade surface, improving the kinematic performance of the machining process, reducing multi-axis coordinated motion control complexity, and improving machining quality. The proposed method was then compared with three traditional methods. The influence of the tool-path on the kinematic performance of the machine tool was quantitatively examined based on the kinematics models of two different machine tools. A large cutting depth milling experiment was conducted to verify that kinematics optimization could improve machining quality. The proposed method provides a more reasonable path-planning approach for blade machining on a five-axis machine tool, which is of great significance in reducing the cost of blade machining and the risks of blade failure. Moreover, it is of great significance for the large-scale automated production of blades.

1. Introduction

The blade is a vital component of turbomachinery, having an important role to play fields as diverse as aerospace, shipbuilding, and new energy. The blade is one of the most widely used free-form surface components and with its complex curvature, its surface quality and profile accuracy are critical to the performance and lifespan of turbomachines [1]. Precision machining of the blade requires a robot or machine tool capable of providing at least five degrees of freedom (DOF) to ensure that the machining tool axis coincides with the normal vector of the blade's surface to maintain a constant contact force and removal [2]. Nowadays, the five-axis machine tool is the first choice for the milling [3], grinding [4], and polishing of a blade, primarily for its high machinability and precision.

Tool-path planning plays a key role in five-axis blade machining. As a typical free-form surface, blade tool-path planning can make use of many existing free-form surface tool-path generation techniques, among which the most commonly used are the iso-parameter [5], iso-planar [6–8], pocketing [9], and iso-cusp height [10–13] methods. The first two methods can be summarized as extending the path along the direction of a constant parameter and offsetting it along another parameter direction so that adjacent parallel paths can be connected end-to-end to generate a continuous machining path. The iso-parameter method is generated with parameters u and v in the parameter domain. The shape of the parameter plane can be regularized to be filled by iso-parameter paths to achieve boundary conformation. Conversely, the iso-planar path is generated with parameters x, y, and z of the Cartesian coordinate system. This method is not designed to be boundary conformed, but it is easier to control the path space. The pocketing method takes the boundary of the surface to be the first path and gradually offsets it inwardly to generate other paths, making it naturally boundary conformed. The iso-cusp height method maintains a constant cusp height between the neighboring tool contact paths. This method is designed based on a specific machining requirement, but it is also not boundary conformed. Many other methods are designed to meet

specific machining requirements, including optimized machining efficiency [14], collision avoidance [15], machine tool kinematics and dynamics characteristics [16], amongst others.

Generally, tool-path planning can be divided into four steps—that is, determining the path direction, planning the tool posture, setting the path space, and setting the step size. Traditional path optimization research has focused on the last three items, optimizing the step size, path spacing, and tool posture based on the requirements of various machining methods. The path direction is often selected based on the characteristics of the surface. As the shapes of free-form surfaces are so different no path-planning method can adapt to all surfaces, and it can be difficult to quantitatively optimize the path direction. However, for free-form parts with specific shape features and specific machining requirements, a path that conforms to its shape characteristics can significantly improve the machining results. A blade surface has similar shape characteristics, surrounded by a flat upper surface (back, pressure surface), a lower surface (abdomen, suction surface), and curved leading (inlet) and trailing (exhaust) edges, the machining difficulty being concentrated on the curved leading and trailing edges (LTE). The profile accuracy of the LTEs has a significant impact on the aerodynamic performance of the blade. Moreover, because the blade working environment is harsh, any stress concentration problem caused by machining defects—such as overcutting, undercutting, or surface corrugation—greatly reduces the service life of the blade and increases the risk of accidents. More than 80% of blade failures originate from machining defects in these areas [17, 18]. However, due to their complex curvature and poor rigidity, LTE areas are also the most difficult areas to machine. Researchers have conducted studies from the perspective of contact force control [19], process parameter adjustment [20], and trajectory parameter optimization [21, 22] to improve LTE machining accuracy. However, the influence of tool-path planning on the machining of the LTEs of blades is rarely discussed.

Zhang [23] proposed an optimized removal strategy for the LTEs to strengthen control of the contact force and removal, suggesting that frequent and large-scale adjustments of the tool posture would reduce machining accuracy and efficiency. Therefore, the longitudinal path (along the length direction of the blade) was found to be more suitable for LTE area machining than the transverse path (along the airfoil direction). However, the study did not explain how to generate longitudinal paths that conformed to LTE features, nor did it quantitatively analyze the impact of two path types it examined on the kinematic performance of machine tools. Wu [24] divided the main body of the blade into four regions based on the curvature and generated paths, respectively, which was similar to the path-planning methods of die-type free-form surfaces. However, Huai [25] suggested that regional division could not be implemented for blade surfaces because machining traces at the boundaries between regions could be quite obvious, causing stress concentration. Zhang [26] suggested that to maintain good aerodynamic performance, one critical machining requirement for blades was that the tool-path should be boundary conformed.

In summary, the tool-path for blade LTE area machining should have three requirements:

- It should be boundary conformed to avoid the gap of the fractal area.
- It should have a uniform path space to avoid stress concentration.

- It should conform to the surface characteristics to reduce tool posture changes.

Traditional path-planning methods struggle to meet all of the above requirements at the same time. In this paper, a new iso-parameter path-planning method was proposed, the paths being generated based on a novel parameterization method combined with the conformal transformation theory. The path could pass through points with similar curvature characteristics on each blade section, avoiding frequent tool posture adjustments in the LTE area, thereby improving the kinematic performance of the blade machining. The influence of different tool-paths on the kinematic performance of the machining tool was quantified based on kinematics models of them. The impact of improved kinematics optimization on the machining results was verified experimentally. The proposed method aims to reduce the difficulty of blade machining and the possibility of machining defects by tool-path optimization, thereby contributing to large-scale automated blade productio.

2. Methodology: Tool-path Planning Methods

2.1 Traditional tool-path planning methods

Planning tool-paths on free-form surfaces is a widely discussed subject, the most commonly used methods being the iso-parameter, iso-planar, and pocketing methods. Fig. 1 shows three traditional path-planning methods. The iso-planar path consists of the intersections of the workpiece surface and a set of parallel cutting planes, the path space being easily controllable. However, the path is not designed to be boundary conformed, and it can be difficult to adapt to the surface curvature characteristics. The iso-parameter path and the pocketing path are generated on the parameter plane, having inherently boundary-conformed characteristics. The coordinates of the blade data points on the parameter plane can be calculated based on the chord length accumulation method. For the data point $P_{i,j}$, the parameter value $v_{i,j}$ can be calculated using:

$$v_{i,j} = \frac{l_i}{L}$$

1

where l_i is the vertical distance from the section plane of point $P_{i,j}$ to the starting end plane, and L is the total length of the blade. The parameter value $u_{i,j}$ is the cumulative chord length parameter of the section airfoil, which can be calculated using [27]:

$$\begin{cases} u_{0,j} = 0 \\ u_{i,j} = u_{i-1,j} + \| \end{cases}$$

2

Based on the three-dimensional coordinates and parameter coordinates of the data points, the C~2 continuous reconstruction surfaces can be established by using the B-spline fitting method. Any point on

the parameter plane can uniquely correspond to a three-dimensional coordinate point on the reconstruction *B*-spline surface. Consequently, the path on the parameter plane can be mapped on the reconstruction surface.

These traditional path-generation methods only consider the uniform distribution of paths on the surface based on geometry. However, the factors restricting path planning in machining are far more complex. A common disadvantage of traditional paths is that they cannot conform to the curvature of the surface. Fig. 2 shows the surface normal vectors on three kinds of paths. When a traditional path passes through the large curvature area of the blade surface, the normal vector of the points on the path changes rapidly. In most machining methods, a specific angle is required between the tool and the surface normal to control the removal volume and shape. Frequent changes of the normal vector of the path mean that the tool must adjust its posture, requiring the machine tool to provide large concomitant movements, resulting in poor kinematics and machining accuracy.

2.2 Parameterization based on conformal transformation

In the path-planning method, the path is often extended along one direction and offset in a fixed direction to generate a trajectory pattern that evenly covers the curved surface. For example, in the longitudinal iso-planar method the path is extended along the *Y-Z* plane and offset in the *X* coordinate direction. Consequently, each point on the same path has the same parameter *x*. The path-planning method can generate a path based on one parameter, such a parameter being the principal parameter of this method —that is, parameter *u* is the principal parameter of the longitudinal iso-parameter path and parameter *v* is the principal parameter of the transverse iso-parameter path. Thus, the reason traditional path-planning methods cannot adapt to the curvature of the surface is that there is no connection between their principal parameters and the curvature. Conversely, a path constructed by a parameter related to the curvature can completely solve this problem.

Conformal transformation is a mathematical algorithm used to map an area of one plane to another plane, maintaining the detailed shape of infinitesimal elements [28]. Conformal transformation theory is widely used in surface parameterization, fluid analysis [29, 30], and airfoil design [31, 32]. As a conformal transformation, the Joukowski transformation can transform a circle on the complex plane, Z_c, into a blade section airfoil on another complex plane, ς, as follows:

\varsigma =f({z_c})={z_c}+{a^2}/{z_c}
3
Thus, an airfoil curve in the rectangular coordinate can be transformed from a circle in polar coordinates as follows:

\left\{ \begin{gathered} x=(\rho +\frac{{{a^2}}}{\rho })\cos \theta \hfill \\ y=(\rho - \frac{{{a^2}}}{\rho })\sin \theta \hfill \\ \end{gathered} \right.
4

where x and y are coordinates of the rectangular coordinate plane, ρ and θ are coordinates of the polar coordinate plane, and a is 1/4 of the airfoil chord length (the length from the leading edge to the trailing edge).

However, an airfoil designed using aerodynamics is not completely consistent with an airfoil obtained using a mathematical transformation. Theodorsen pointed out that when the airfoil is converted from a rectangular coordinate plane to a polar coordinate plane, a quasi-circular curve is usually obtained, which can be expressed as follows:

$$z_c=a\rho (\theta)\exp (i\theta)$$
5
where θ is the polar angle and$\rho (\theta)$is the polar radius of the quasi-circle, which is close to being a constant. Substituting Eq. (5) into Eq. (4):

$$\left\{ \begin{gathered} x=a(\rho +\frac{1}{\rho })\cos \theta \hfill \\ y=a(\rho - \frac{1}{\rho })\sin \theta \hfill \\ \end{gathered} \right.$$
6
where ρ and θ can be solved as follows:

$$\begin{gathered} {\sin ^2}\theta =\frac{1}{2}(h+\sqrt {{h^2}+\frac{{{y^2}}}{{{a^2}}}}) \hfill \\ \rho =\frac{1}{{2a}}(\frac{x}{{\cos \theta }}+\frac{y}{{\sin \theta }}) \hfill \\ \end{gathered}$$
7
where,$h=\frac{{ - {x^2} - {y^2}+4{a^2}}}{{4{a^2}}}$.
As shown in Fig. 3, based on Eq. (7), the airfoil in the rectangular coordinate system can be converted into a quasi-circle in the polar coordinate system. The quasi-circular polar angle, θ, uniquely corresponds to the data point on the airfoil and is related to the curvature, making it a good principal parameter for longitudinal path planning on the blade surface.

Figure 4 shows the relationship between the curvature, k, and the principal parameters of different path-planning methods. Asterisks mark the trailing edges of the blade section profiles, the dashed line indicating the principal parameter and the corresponding path generated on the surface. There is no correlation between the parameters u or x and the curvature. Their paths traverse the different curvature areas of each section irregularly. There is no correlation between the parameter u or x and the curvature, so the paths ignore the curvature characteristics of the surface and bypass the large curvature area, resulting in a rapid change of the surface normal vector on the path. However, the quasi-circle polar angle, θ, shows a strong correlation with the curvature. The paths pass through points with similar curvature characteristics on each section. For example, the highlighted path starts from the trailing edge of the first section and passes through the trailing edges of each section. Consequently, it is not affected by the curvature of the airfoil and always passes through the LTE area along the direction of small curvature.

2.3 Path based on conformal transformation of section profile

A new iso-parameter tool-path planning method can be generated using the quasi-circular polar angle, θ, as the principal parameter. The process is shown in Fig. 5, and the procedure can be summarized as follows:

(Procedure 1) Quasi-circle polar angle path-planning method

1) Calculate the parameter *v* of data points using the same method as Eq. (1).

2) Standardize the section airfoils. The farthest two points among the discrete data points of one section are set as the leading edge and trailing edge respectively. The two edges of each airfoil should be placed at the coordinates (−0.5, 0) and (0.5, 0) through coordinate transformation and scaling.
3) Calculate the quasi-circle polar angle, θ, corresponding to each point using conformal transformation as in Eq. (7).
4) Calculate the quasi-circle parameter,{u_\theta }, to be {u_\theta }=\theta /2\pi, so that this parameter can be standardized in the interval of [0,1] as a knot vector.
5) Use the B-spline surface fitting method to generate a reconstruction surface as follows:
S({u_\theta },v)=\sum\limits_{{i=0}}^{n} {\sum\limits_{{j=0}}^{m} {{N_{i,k}}({u_\theta })} } {N_{j,l}}(v){d_{i,j}} 8
where,{d_{i,j}}(i=0,1, \cdots ,n,j=0,1, \cdots ,m) is the control vertex mesh, {N_{i,k}}(u) is the *k*-th B-spline basis function defined by the knot vector \mathbf{U}=({u_{\theta 0}},{u_{\theta 1}}, \cdots ,{u_\theta }_{{n+k}}); and {N_{j,k}}(v) is the *l*-th B-spline basis function defined by the knot vector \mathbf{V}=({v_0}, {v_1}, \cdots ,{v_{m+l}}).

6) Generate iso-parameter paths on the parametric plane. Extend the path along the parameter *v* direction and offset the path along the parameter {u_\theta } direction.

7) Map the parameter paths to the reconstruction surface.
Figure 6 shows the proposed path and the surface normal vector on the path. The proposed path is boundary conformed, evenly distributed, and adapts to the curvature, with little bending or distortion. Compared with the traditional paths, as shown in Fig. 2, there is no rapid change of surface normal vector on the paths near the LTE area. The tool does not need to adjust its posture frequently during machining, which enhances the machining stability, reduces motion control complexity, and improves the kinematics of the machine tool.

3. Kinematics Analysis And Comparison

Free-form surfaces have curvature changes in multiple directions and are prone to interference problems. A fixed angle should be maintained between the tool and the surface normal vector at the contact point. Therefore, blade surface machining requires at least five DOF to adjust the position and posture of the tool including three translation freedoms (3T) and two rotational freedoms (2R), as shown in Fig. 7(a). By assigning specific DOF to different actuators, five-axis machine tools can have many configurations.

However, as shown in Fig. 7(b), regardless of the configuration, when the tool bypasses the large curvature area, it needs to provide huge concomitant movement.

In this section, the kinematics constraint equations of two five-axis machine tools are established. The influence of tool-paths on machine tool kinematics is quantitatively evaluated using the inverse kinematics solution. When the tool is machining along a path, the drive axis displacement changes smoothly at a lower speed, the machine tool kinematic performance being much improved, and the machining having higher stability and motion control accuracy.

3.1 Kinematics constraint equations of two different machine tools

In kinematic analysis, the machine tool can be simplified as a multi-body system that only focuses on the kinematics chain. By establishing a fixed coordinate system on each body, the relative motion between bodies can then be described through coordinate transformation matrixes. The motion constraint equations of different machine tools can be obtained by arranging the coordinate transformation matrixes based on the low-order body array.

Figure 8 shows machine tool I with a serial configuration alongside its structural diagram. The machine tool includes an X-direction guide (1), Y-direction guide (2), polishing tank (3), rotating platform (4), tool rotating platform (6), and Z-direction guide (7). The blade (5) is fixed to the rotating platform (4) and can rotate with it to provide C-direction rotation, \tilde {\gamma }, around the Z-axis. The X-direction guide (1), Y-direction guide (2), and Z-direction guide (7) provide X-direction displacement, \tilde {x}, Y-direction displacement, \tilde {y},and Z-direction displacement, \tilde {z}, respectively. The tool rotation platform (6) provides B-direction rotation, \tilde {\beta }, about the Y-axis.

The kinematics constraint equation of the machine tool can be expressed as follows:

\left[{\begin{array}{*{20}{c}} { - r} \\ 0 \\ { - R} \\ 1 \end{array}} \right]=\left[{\begin{array}{*{20}{c}} {\cos (\tilde {\beta })}&0&{ - \sin (\tilde {\beta })}&0 \\ 0&1&0&0 \\ {\sin (\tilde {\beta })}&0&{\cos (\tilde {\beta })}&0 \\ 0&0&0&1 \end{array}} \right] \bullet \left[{\begin{array}{*{20}{c}} 1&0&0&{ - {x_l}} \\ 0&1&0&{ - {y_l}} \\ 0&0&1&{ - \tilde {z} - {z_l}} \\ 0&0&0&1 \end{array}} \right] \bullet \left[{\begin{array}{*{20}{c}} 1&0&0&{\tilde {x}} \\ 0&1&0&{\tilde {y}} \\ 0&0&1&0 \\ 0&0&0&1 \end{array}} \right] \bullet \left[{\begin{array}{*{20}{c}} {\cos (\tilde {\gamma })}&{ - \sin (\tilde {\gamma })}&0&0 \\ {\sin (\tilde {\gamma })}&{\cos (\tilde {\gamma })}&0&0 \\ 0&0&1&0 \\ 0&0&0&1 \end{array}} \right] \bullet \left[{\begin{array}{*{20}{c}} 0&0&1&0 \\ {-1}&0&0&0 \\ 0&1&0&0 \\ 0&0&0&1 \end{array}} \right] \bullet \left[{\begin{array}{*{20}{c}} x \\ y \\ z \\ 1 \end{array}} \right]

10

where (x, y, z) is the position of the tool contact point in the blade coordinate system, (x_l, y_l, z_l) is the position of the origin, O_t, of the tool rotation platform coordinate system on the machine coordinate

system, R is the distance from the end of the tool to O_t, and r is the tool radius. The axes movement position can be obtained from the inverse kinematics solution of the tool position and posture, as follows:

$$\begin{cases} \tilde{\gamma} = \arctan 2(P_y / P_x) \\ \tilde{\beta} = \arctan 2(\|P_x + P_y\| / P_z) \\ \tilde{x} = -x\cos(\tilde{\gamma})\cos(\tilde{\beta}) + y\sin(\tilde{\gamma})\cos(\tilde{\beta}) - z\sin(\tilde{\beta}) \\ \tilde{y} = -x\sin(\tilde{\gamma}) - y\cos(\tilde{\gamma}) \\ \tilde{z} = x\cos(\tilde{\gamma})\sin(\tilde{\beta}) - y\sin(\tilde{\gamma})\sin(\tilde{\beta}) - z\cos(\tilde{\beta}) \end{cases} \quad (11)$$

where (P_x, P_y, P_z) is the tool vector.

Figure 9 shows machine tool II with a hybrid configuration alongside its structural diagram. The machine tool includes a base (0), Y-direction guide (1), fixed platform (2), 3-RPS parallel motion platform (3), rotating fixture (4), X-direction guide (5), abrasive belt tool (6), and clamper (7). The clamper (7) fixes the blade to the rotating fixture (4), which provides B-direction rotation, \tilde {\beta }, around the Y-axis. The X-direction guide (5) and Y-direction guide (1) provide X-direction displacement, \tilde {x}, and Y-direction displacement, \tilde {y}, respectively. The 3-RPS parallel motion platform (3) locks the rotation freedom around the Y-axis, only providing Z-direction displacement, \tilde {z}, and A-direction rotation around the X axis.

The kinematics constraint equation can be expressed as follows:

\left[{\begin{array}{*{20}{c}} {{x_t}} \\ {{y_t}} \\ {{z_t}} \\ 1 \end{array}} \right]=\left[{\begin{array}{*{20}{c}} 1&0&0&{ - \tilde {x}} \\ 0&1&0&0 \\ 0&0&1&0 \\ 0&0&0&1 \end{array}} \right] \bullet \left[{\begin{array}{*{20}{c}} 1&0&0&0 \\ 0&1&0&{\tilde {y}} \\ 0&0&1&0 \\ 0&0&0&1 \end{array}} \right] \bullet \left[{\left[{\begin{array}{*{20}{c}} 1&0&0&{{x_p}} \\ 0&{\cos (\tilde {\alpha })}&{ - \sin (\tilde {\alpha })}&{r\cdot (1 - \cos (\tilde {\alpha }))+{y_p}} \\ 0&{\sin (\tilde {\alpha })}&{\cos (\tilde {\alpha })}&{ - {z_p} - \tilde {z}} \\ 0&0&0&1 \end{array}} \right]} \right]\left[{\begin{array}{*{20}{c}} {\cos (\tilde {\beta })}&0&{\sin (\tilde {\beta })}&{{x_r}} \\ 0&1&0&{{y_r}} \\ { - \sin (\tilde {\beta })}&0&{\cos (\tilde {\beta })}&{{z_r}} \\ 0&0&0&1 \end{array}} \right] \bullet \left[{\begin{array}{*{20}{c}} x \\ y \\ z \\ 1 \end{array}} \right]

12

where (x, y, z) is the position of the tool contact point in the blade coordinate system, (x_r, y_r, z_r) is the position of the origin, O_b, of the blade coordinate system on the motion platform coordinate system, (x_p, y_p, z_p) is the position of the origin, O_m, of the motion platform coordinate system on the fixed platform coordinate system in the initial state, and (x_t, y_t, z_t) is the position of the tool nose on the machine coordinate system in the initial state. \tilde {z} and \tilde {\alpha } are coupled by the linear motion of three parallel drive axes, which can be calculated as follows:

\begin{gathered} {L_1}{\text{=}}\sqrt {{{(\frac{3}{2} \bullet {r_b} \bullet \cos (\tilde {\alpha }) - \frac{1}{2} \bullet {r_b} - {r_p})}^2}+{{(- {r_b} \bullet \sin (\tilde {\alpha })+z+\tilde {z})}^2}} \hfill \\ {L_2}{\text{=}} {L_{\text{3}}}{\text{=}}\sqrt {{{({r_b} - {r_p})}^2}+{{(\frac{1}{2} \bullet {r_b} \bullet \sin (\tilde {\alpha })+z+\tilde {z})}^2}} \hfill \\ \end{gathered}
13
where {r_b} and {r_p} are the distances from the center of the motion platform and the fixed platform to the hinge point, respectively.

3.2 Kinematics analysis of the tool-paths

Based on the inverse kinematics solution, the machine tool drive axes displacement of traditional paths is as shown in Fig. 10. Although the configurations differ, the two machine tools show similar kinematic characteristics. In the large curvature area where the surface normal vector changes rapidly, the kinematic characteristics of the machine tool deteriorate. The displacement of multiple drive axes related to the tool posture adjustment changes rapidly over a small range, which is differs significantly from the displacement of a flat area. When machining this area, the drive axes need not only high-speed motion but also rapid acceleration. Multi-axis dynamic coordination is required to ensure the accuracy of tool movement, which increases the difficulty of machine tool control and the probability of machining defects. The transverse and pocket paths extend along the direction of the blade, and unavoidable tool posture adjustment is required. However, two longitudinal paths extending along the length direction still cannot avoid this problem in key areas, as the paths cannot adapt to the surface curvature.

In the proposed method, this problem is completely solved. Fig. 11 shows the machine tool drive axes displacement of the proposed path. In the trailing-edge area—with its complex curvature—the axis displacement still changes smoothly without any rapid variations. Compared with the traditional paths near the trailing-edge area, the axis rotation is reduced by 90%, and the axis motion by 60%.

When the feed rate is constant at 500 mm/min, the axis motion speed is as shown in Fig. 12. The kinematic characteristics of the pocket path are similar to those of the transverse path, so they need no longer be compared. Among the three comparison methods, the longitudinal iso-parametric path is the least affected by the tool posture adjustment. The maximum rotation and motion speeds of the proposed path are only 1.2% and 10% of the longitudinal iso-parametric path, respectively. Concomitant movement in the LTE area is reduced by 98%. The speed of the axis is much lower than comparison methods, which improves the kinematic characteristics of the machining.

Suppose the speed limit of the linear axis is 100 mm/s, and the speed limit of the rotary axis is 30°/s. The maximum speed that the tool can reach under the axis limit is as shown in Fig. 13. In the traditional paths, the tool feed speed is restricted in the LTE area, reducing the machining efficiency and causing uneven removal. In the proposed path, the feed speed limit is always close to the speed limit of the linear axis and is not restricted by the concomitant motion axis, so it has excellent kinematic characteristics. The minimum feed speed is four times that of the traditional longitudinal iso-parametric path.

4. Experimental Results

Kinematics analysis showed that the proposed path-planning method could significantly improve the kinematic characteristics of blade machining. In this section, the machining improvement due to kinematics optimization was verified experimentally. A five-axis machine tool was used to mill aero-engine blades along different paths with a large cutting depth and a high feed speed. The machining results were evaluated based on the accuracy of the milling traces and the uniformity of the removal depth.

We imported several paths into the UG NX software application in the form of discrete points to generate CAM machining files. The built-in post-machining system of the machine tool could compile this file to generate control code. The cutting depth was set to be 0.2 mm and the feed speed of the tool was constant at 500 mm/min. The large cutting depth and high feed speed placed higher requirements on the motion control ability of the machine tool, making it easier to find machining defects during the experiment. The comparison paths included transverse, longitudinal iso-parametric, and longitudinal iso-planar paths. Each path-planning method selected one path close to the LTE area that was prone to machining defects. The proposed path was evenly distributed on the surface in a parallel raster form. The experiment was repeated three times. The milling process and milling traces are as shown in Fig. 14.

In the experiment, to control the influence of other factors on the machining accuracy, the machining and blade experiment were completed in one clamping. The chord error was set to 0.001 mm—which was much smaller than the cutting depth—to eliminate interpolation errors. Path planning and blade machining were based on the same model, so there was no path matching error. As the influence of path matching, interpolation, and clamping errors had been eliminated, the machining defects were due to inaccurate multi-axis coordinated motion. Poor kinematics is the primary reason it is difficult for the machine tool motion control system to achieve multi-axis coordinated motion accurately.

The Keyence ultra-depth-of-field microscope and Taylor contact stylus profiler were used to observe the milling traces and measure the removal depth, as shown in Fig. 15.

The observation and measurement results of the comparison paths are shown in Fig. 16. Fig. 16(a) shows the measurement results of four areas on the transverse path. Area 1 and Area 3 are on the flat part of the blade, and the cutting depths meet requirements. The cutting depths of Area 2 and Area 4 in the LTE area are inaccurate, causing overcutting and undercutting problems. The cutting depth measurement results of 20 areas along the traces of three experiments are also shown.

The overcut and undercut areas are all located in the LTE area. Fig. 16(b) shows the measurement results of four areas on the longitudinal iso-parameter path. The undercutting problem occurs in Area 2 and Area 3, which are also located in the LTE area. Fig. 16(c) shows the measurement results of three areas on the longitudinal iso-planar path, which is near the leading edge. No serious overcutting or undercutting problems were found. However, in Area 1, there is an obvious path distortion. Combining the drive axis displacements in Fig. 10 it can be seen that there is a close correlation between machining defects and

rapid changes of displacement. In the transverse and the longitudinal iso-parameter paths, the Z-axis—which controls the milling depth—bears the largest concomitant motion, moving rapidly in the LTE area, overcut and undercut defects appearing on both paths. In the iso-planar path, the Y-axis bears the largest concomitant motion, which is also the axis that causes path distortion. It can be shown that axes with poor kinematics are more prone to machining defects.

Figure 17 shows the measurement results of milling traces of the proposed path. The cutting depth on multiple traces are all close to the expected depth of 0.2 mm. No overcutting or undercutting problems were found. The average cutting depths and the standard deviations of all experiments are shown in Table 1. Compared with the traditional longitudinal iso-parametric path, the maximum deviation of the cutting depth is reduced by 90%, and the standard deviation is by 70%.

Table 1
The cutting depth of the experimental results

		Transverse path	Longitudinal iso-planar path	Longitudinal iso-parametric path	The proposed path
Experiment 1	Average cutting depth (μm)	200.5	201.2	195.3	200.1
	Standard deviation (μm)	25.5	6.7	19.6	2.9
Experiment 2	Average cutting depth (μm)	206.7	200.6	194.4	199.7
	Standard deviation (μm)	17.4	5.6	18.5	2.9
Experiment 3	Average cutting depth (μm)	201.3	201.7	207.8	199.9
	Standard deviation (μm)	16.3	6.2	15.6	3.1

The experimental results showed that the kinematics optimization of the proposed path could improve the quality of the blades processed using the five-axis machine tool and reduce machining defects. This improvement was attributed to the fact that the proposed path could adapt to the curvature characteristics of the blade, which could be applied to different machine tool configurations and machining methods. The proposed path reduces the difficulty of blade machining, so that a low-precision five-axis machine tool without a force servo control system can avoid machining defects in the LTE area, thereby reducing the cost of blade machining and the risks of blade failure.

5. Conclusions

A new iso-parametric path-planning strategy for a blade free-form surface based on a novel parameterization method combined with conformal transformation was proposed. The proposed method

could adapt to the curvature characteristics of the blade surface, thus simultaneously meeting the three requirements of blade machining—that is, it should be boundary conformed, have uniform distribution, and small tool posture changes. Compared with traditional paths, the proposed path was smoother and straighter, without bending or twisting in the LTE area, thus avoiding frequent adjustments of the tool machining posture.

The influence of different tool-paths on the kinematic performance was quantitatively examined based on the kinematics models of two machine tools with different configurations. Compared with the traditional iso-parameter longitudinal path—which had the best kinematic performance of the traditional paths—the maximum rotation speed of the proposed path in the LTE area was reduced by 98%, the concomitant motion speed was reduced by 98%, which in turn reduced the maximum linear speed by 90%. The feed speed of the tool could reach the axis speed limit without mechanical restriction, reaching four times that of the traditional path in the LTE area.

A large cutting depth milling experiment was conducted to verify machining quality improvements due to the kinematics optimization. Several machining defects were found on the milling traces of the traditional paths, due to insufficient accuracy of the multi-axis coordinated motion caused by poor kinematic performance. Under the same machining conditions, the proposed path did not show any machining defects and reduced the maximum deviation of cutting depth by 90% and the standard deviation by 70%.

The proposed method provides a more reasonable path-planning method for blade machining based on kinematics optimization. This improvement can be attributed to the fact that the proposed path could adapt to the curvature characteristics of the blade, which can be applied to different machine tool configurations and machining methods. The proposed path reduces the difficulties involved in blade machining, so that low-precision five-axis machine tools without a force servo control system can avoid machining defects in the LTE area, thereby reducing the cost of blade machining and the risk of blade failure. This is of great significance for the large-scale automated production of blades.

Declarations

Acknowledgement

The authors would like to be grateful to a grant from the National Natural Science Foundation of China (Grant No. 51135006,52175538).

Funding The authors would like to be grateful to a grant from the National Natural Science Foundation of China (Grant No. 51135006,52175538).

Conflict of Interest This manuscript has not been published or presented elsewhere in part or in entirety and is not under consideration by another journal. There are no conflicts of interest to declare.

Authors' contributions：Zhongyang Lu: Methodology, Visualization, Data curation, Validation, Writing and Editing；Xu Yang: Conceptualization, Editing and Supervision；Ji Zhao: Supervision.

References

1. Chen H, Yu W, Capellaro M (2010) A critical assessment of computer tools for calculating composite wind turbine blade properties. Wind Energy 13:497–516
2. Xu X, Chen W, Zhu D, Yan S, Ding H (2021) Hybrid active/passive force control strategy for grinding marks suppression and profile accuracy enhancement in robotic belt grinding of turbine blade. Robot Comput Integr Manuf 67:102047
3. Huang N, Bi Q, Wang Y, Sun C (2014) 5-Axis adaptive flank milling of flexible thin-walled parts based on the on-machine measurement. Int J Mach Tools Manuf 84:1–8
4. Khan AW, Wuyi C (2010) Systematic geometric error modeling for workspace volumetric calibration of a 5-axis turbine blade grinding machine. Chin J Aeronaut 23:604–615
5. Elber G, Cohen E (1994) Toolpath generation for freeform surface models. Comput Aided Des 26:490–496
6. Suh YS, Lee K (1990) NC milling tool path generation for arbitrary pockets defined by sculptured surfaces. Comput Aided Des 22:273–284
7. Ding S, Mannan M, Poo AN, Yang D, Han Z (2003) Adaptive iso-planar tool path generation for machining of free-form surfaces. Comput Aided Des 35:141–153
8. Feng H-Y, Teng Z (2005) Iso-planar piecewise linear NC tool path generation from discrete measured data points. Comput Aided Des 37:55–64
9. Xu K, Tang K (2014) Five-axis tool path and feed rate optimization based on the cutting force–area quotient potential field. The International Journal of Advanced Manufacturing Technology 75:1661–1679
10. Lee E (2003) Contour offset approach to spiral toolpath generation with constant scallop height. Comput Aided Des 35:511–518
11. Can A, Ünüvar A (2010) A novel iso-scallop tool-path generation for efficient five-axis machining of free-form surfaces. The International Journal of Advanced Manufacturing Technology 51:1083–1098
12. Yoon J-H (2005) Fast tool path generation by the iso-scallop height method for ball-end milling of sculptured surfaces. Int J Prod Res 43:4989–4998
13. Lo C-C (1999) Efficient cutter-path planning for five-axis surface machining with a flat-end cutter. Comput Aided Des 31:557–566
14. Chiou C-J, Lee Y-S (2002) A machining potential field approach to tool path generation for multi-axis sculptured surface machining. Comput Aided Des 34:357–371
15. Jun C-S, Cha K, Lee Y-S (2003) Optimizing tool orientations for 5-axis machining by configuration-space search method. Comput Aided Des 35:549–566

16. Wang N, Tang K (2008) Five-axis tool path generation for a flat-end tool based on iso-conic partitioning. Comput Aided Des 40:1067–1079
17. Vardar N, Ekerim A (2007) Failure analysis of gas turbine blades in a thermal power plant. Eng Fail Anal 14:743–749
18. Mazur Z, Luna-Ramirez A, Juárez-Islas J, Campos-Amezcua A (2005) Failure analysis of a gas turbine blade made of Inconel 738LC alloy. Eng Fail Anal 12:474–486
19. Liu ZY, Huang Y, Wei HP, Sun C (2013) Research on the technology of NC abrasive belt grinding for the leading and trailing edges of aero-engine blades,Advanced Materials Research, Trans Tech Publ, pp.67–72
20. Zhang J, Shi Y, Lin X, Li Z (2017) Parameter optimization of five-axis polishing using abrasive belt flap wheel for blisk blade. J Mech Sci Technol 31:4805–4812
21. Huai W, Shi Y, Tang H, Lin X (2017) Sensitivity of surface roughness to flexible polishing parameters of abrasive cloth wheel and their optimal intervals. J Mech Sci Technol 31:865–873
22. Wei W, Chao Y (2011) A path planning method for robotic belt surface grinding. Chin J Aeronaut 24:520–526
23. Zhang J, Shi Y, Lin X, Li Z (2017) Five-axis abrasive belt flap wheel polishing method for leading and trailing edges of aero-engine blade. The International Journal of Advanced Manufacturing Technology 93:3383–3393
24. Xuan W, Yonglin C (2017) The tool path planning of Composed Surface of Big-twisted Blisk. Procedia Eng 174:392–401
25. Huai W, Shi Y, Tang H, Lin X (2019) An adaptive flexible polishing path programming method of the blisk blade using elastic grinding tools. J Mech Sci Technol 33:3487–3495
26. Zhang R, Hu P, Tang K (2015) Five-axis finishing tool path generation for a mesh blade based on linear morphing cone. Journal of Computational Design and Engineering 2:268–275
27. Piegl L, Tiller W (2012) The NURBS book. Springer Science & Business Media
28. Abbott IH, Von AE, Doenhoff (2012) Theory of wing sections: including a summary of airfoil data. Courier Corporation
29. Bai C, Li J, Wu Z (2014) Generalized Kutta–Joukowski theorem for multi-vortex and multi-airfoil flow with vortex production — A general model. Chin J Aeronaut 27:1037–1050
30. Bai C, Wu Z (2014) Generalized Kutta–Joukowski theorem for multi-vortex and multi-airfoil flow (a lumped vortex model). Chin J Aeronaut 27:34–39
31. Chen H, Jaworski JW (2020) Aeroelastic interactions and trajectory selection of vortex gusts impinging upon Joukowski airfoils. J Fluids Struct 96:103026
32. Parakkal JU, Kadi KE, El-Sinawi A, Elagroudy S, Janajreh I (2019) Numerical analysis of VAWT wind turbines: Joukowski vs classical NACA rotor's blades. Energy Procedia 158:1194–1201

Figures

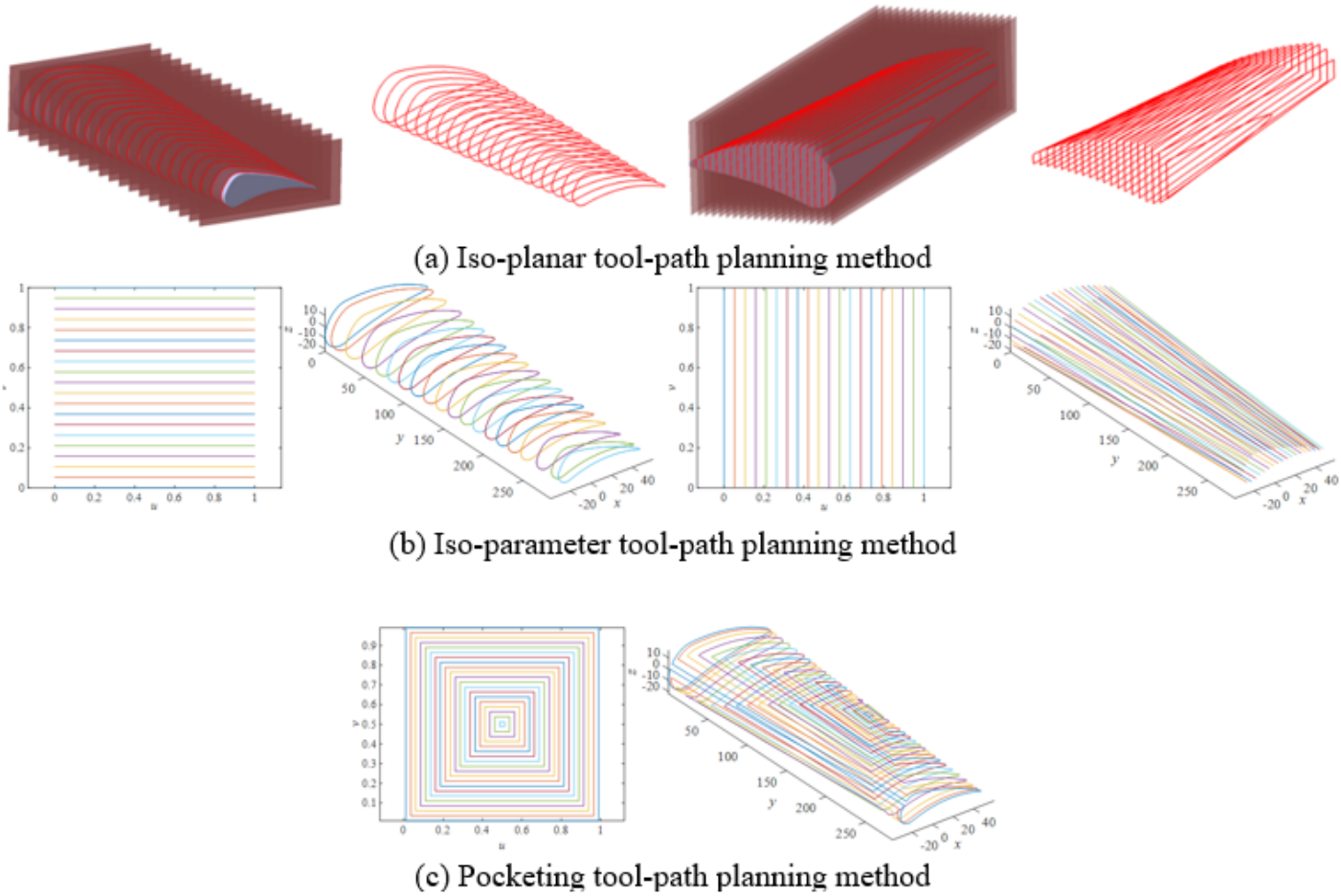

Figure 1

Traditional tool-path planning methods

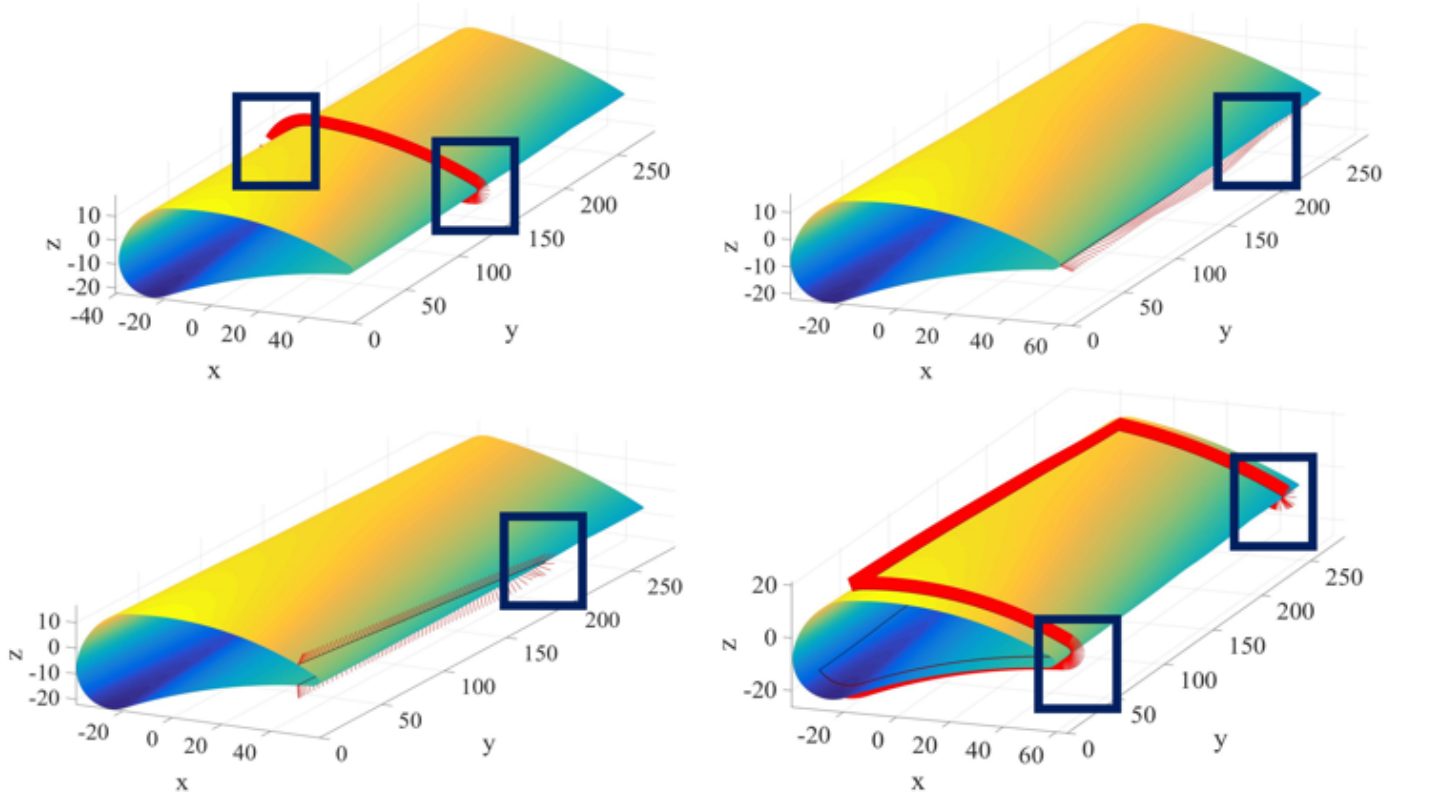

Figure 2

Position where the surface normal vector changes rapidly on a traditional path

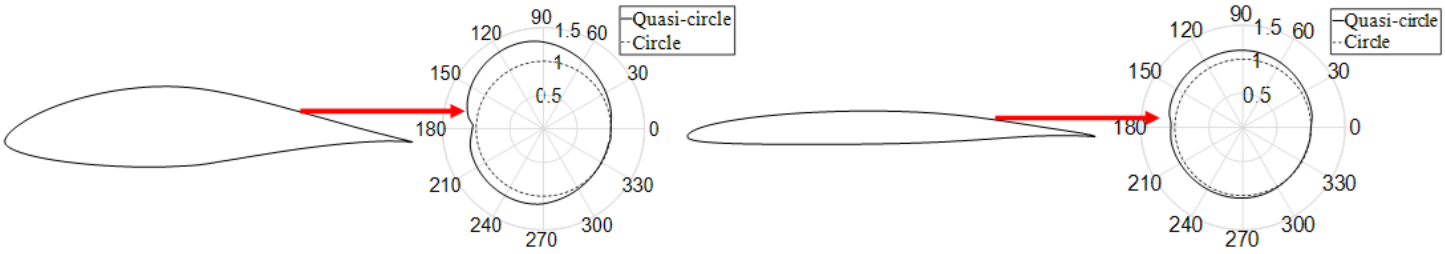

Figure 3

Conformal transformation

Figure 4

Relationship between curvature and principal parameters

Figure 5

Quasi-circle polar angle path-planning method

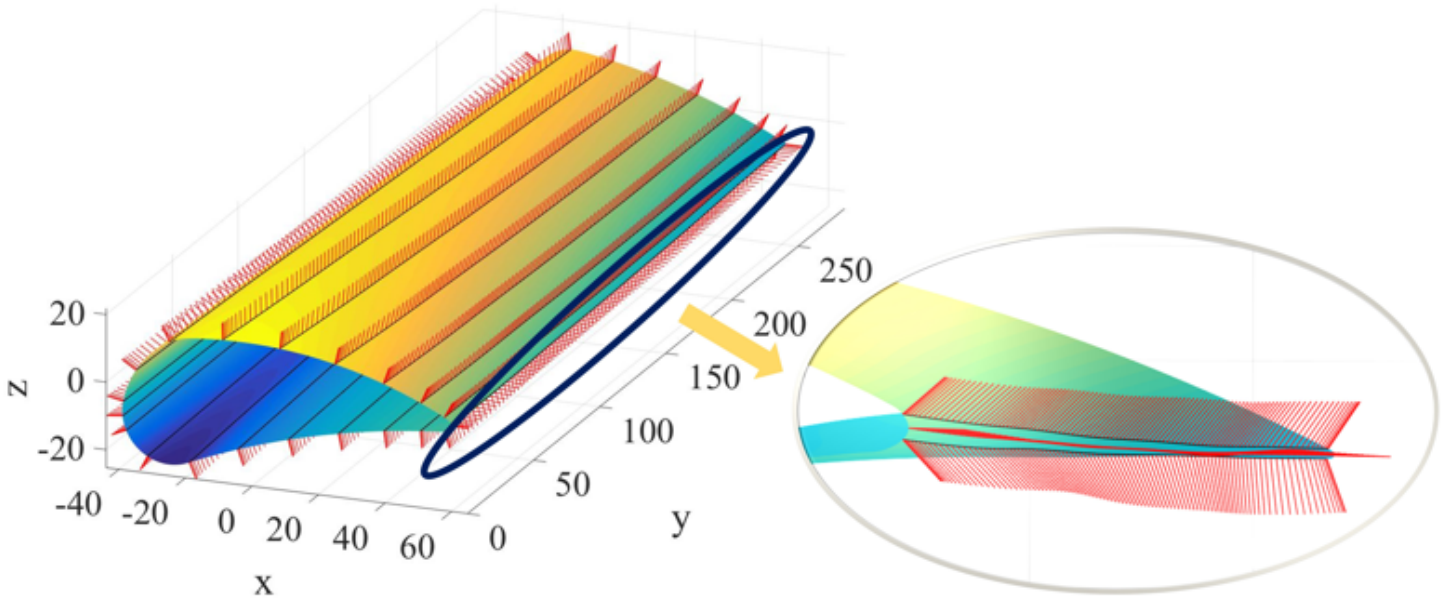

Figure 6

Quasi-circle polar angle path

Figure 7

Blade machining requirements and machine tool configurations

Figure 8

Machine tool I with a serial configuration

Figure 9

Machine tool II with a hybrid configuration

Figure 10

Machine tool drive axes displacement of the traditional paths

Figure 11

Machine tool drive axes displacement of the proposed path

Figure 12

Machine tool drive axes speed of different paths

Figure 13

Speed constraints of different tool-paths

Figure 14

Milling experiment and milling traces

Figure 15

Milling trace observation and measurement equipment

Figure 16

The experimental results of the traditional methods

Figure 17

The experimental results the proposed method